Available online at www.sciencedirect.com
SCIENCE DIRECT
Thermochimica Acta 436 (2005) 101–112
thermochimica acta
www.elsevier.com/locate/tca

Role of isoconversional methods in varying activation energies of solid-state kinetics II. Nonisothermal kinetic studies

Ammar Khawam *, Douglas R. Flanagan

Division of Pharmaceutics, College of Pharmacy, University of Iowa, Iowa City, IA 52242, USA

Received 21 February 2005; received in revised form 17 May 2005; accepted 17 May 2005
Available online 28 June 2005

Abstract

The concept of variable activation energy in solid-state reaction kinetics has caused considerable debate. Activation energy variation has been detected by isoconversional or "model-free" calculation methods, which generate activation energy as a function of reaction progress. The relationship between calculation methods and artifactual variation in activation energy was investigated in this work by employing model-fitting and isoconversional methods to analyze both simulated and experimental nonisothermal data. The experimental data was for nonisothermal sulfameter-dioxolane solvate desolvation by TGA. We show that variable activation energy in simple reactions could be an artifact resulting from the incorrect application of isoconversional methods.

Keywords: Solid-state kinetics; Isothermal kinetics; Nonisothermal kinetics; Activation energy; Arrhenius equation; Desolvation; Sulfameter; Isoconversion; Model-fitting; Model-free

1. Introduction

Some theoretical aspects of solid-state kinetics have caused numerous debates and controversies [1,2]. One such controversy is the variation in activation energy as a function of reaction progress [3,4]. Explanations for this variation usually focus on the complexities inherent in solid-state kinetics with little consideration being given to secondary effects, such as artifacts from mathematical or computational methods. The aim of this work is to test the reliability of these methods. Our previous work focused on analyzing isothermal data [5] and this part focuses on kinetic analysis of simulated and real experimental nonisothermal data.

1.1. Rate laws and kinetic analysis

The rate of a solid-state reaction can be generally described by,

$$\frac{d\alpha}{dt} = kf(\alpha) \tag{1}$$

where k is the reaction rate constant, $f(\alpha)$ is the reaction model and α is the conversion fraction.

Integrating the above equation gives the integral rate law,

$$g(\alpha) = kt \tag{2}$$

where $g(\alpha)$ is the integral reaction model. The temperature dependence of the rate constant is described by the Arrhenius equation [6],

$$k = A\, e^{-E_a/RT} \tag{3}$$

* Corresponding author. Tel.: +1 319 335 8819; fax: +1 319 335 9349.
E-mail address: ammar-khawam@uiowa.edu (A. Khawam).

0040-6031/$ – see front matter © 2005 Elsevier B.V. All rights reserved.
doi:10.1016/j.tca.2005.05.015

where A is the pre-exponential (frequency) factor, E_a is the activation energy, T is the absolute temperature and R is the gas constant.

Substituting Eq. (3) in the above rate expressions gives,

$$\frac{d\alpha}{dt} = A\, e^{-E_a/RT} f(\alpha) \tag{4}$$

and

$$g(\alpha) = A\, e^{-E_a/RT} t \tag{5}$$

Several reaction models [7] using $f(\alpha)$ or $g(\alpha)$ are listed in Table 1.

Kinetic parameters can be obtained from isothermal kinetic data by applying these rate laws or can be transformed into nonisothermal rate expressions describing reaction rate as a function of temperature at a constant heating rate by utilizing the following,

$$\frac{d\alpha}{dT} = \frac{d\alpha}{dt}\frac{dt}{dT} \tag{6}$$

where $d\alpha/dT$ is the nonisothermal reaction rate, $d\alpha/dt$ is the isothermal reaction rate and dt/dT is the inverse heating rate ($1/\beta$).

Substituting Eq. (4) into Eq. (6) gives the differential form of the nonisothermal rate law,

$$\frac{d\alpha}{dT} = \frac{A}{\beta} e^{-E_a/RT} f(\alpha) \tag{7}$$

Upon integration, Eq. (7) gives,

$$g(\alpha) = \frac{A}{\beta}\int_0^T e^{-E_a/RT} dT \tag{8}$$

If E_a/RT is replaced by "x" and integration limits transformed, Eq. (8) becomes,

$$g(\alpha) = \frac{AE_a}{\beta R}\int_x^\infty \frac{e^{-x}}{x^2} dx \tag{9}$$

Eq. (9) can be written as,

$$g(\alpha) = \frac{AE_a}{\beta R} p(x) \tag{10}$$

where $p(x)$ is the exponential integral.

The exponential integral ($p(x)$) has no analytic solution [8], but has many approximations [8–12].

Kinetic parameters can be obtained from nonisothermal rate laws by both model-fitting and isoconversional (model-free) methods. Model-fitting methods involve fitting different models to α-temperature curves and simultaneously determining the activation energy (E_a) and frequency factor (A). There are several nonisothermal model-fitting methods, one of the most popular being the Coats and Redfern method [13,14]. This method utilizes the asymptotic series expansion for approximating the exponential integral ($p(x)$) in Eq. (10), giving,

$$\ln\frac{g(\alpha)}{T^2} = \ln\left(\frac{AR}{\beta E_a}\left[1 - \left(\frac{2RT_{exp}}{E_a}\right)\right]\right) - \frac{E_a}{RT} \tag{11}$$

where T_{exp} is the mean experimental temperature.

Plotting the left-hand side of Eq. (11), which includes the model $g(\alpha)$, versus $1/T$ gives E_a and A from the slope and intercept, respectively. The model that gives the best linear fit is selected as the model of choice.

Modelistic methods has been criticized in nonisothermal studies [15–19], because:

Table 1
Solid-state rate expressions for different reaction models

Model	Differential form $f(\alpha) = \frac{1}{k}\frac{d\alpha}{dt}$	Integral form $g(\alpha) = kt$
Nucleation models		
Power law (P2)	$2\alpha^{(1/2)}$	$\alpha^{(1/2)}$
Power law (P3)	$3\alpha^{(2/3)}$	$\alpha^{(1/3)}$
Power law (P4)	$4\alpha^{(3/4)}$	$\alpha^{(1/4)}$
Avarami-Erofe'ev (A2)	$2(1-\alpha)[-\ln(1-\alpha)]^{1/2}$	$[-\ln(1-\alpha)]^{1/2}$
Avarami-Erofe'ev (A3)	$3(1-\alpha)[-\ln(1-\alpha)]^{2/3}$	$[-\ln(1-\alpha)]^{1/3}$
Avarami-Erofe'ev (A4)	$4(1-\alpha)[-\ln(1-\alpha)]^{3/4}$	$[-\ln(1-\alpha)]^{1/4}$
Geometrical contraction models		
Contracting area (R2)	$2(1-\alpha)^{1/2}$	$[1-(1-\alpha)^{1/2}]$
Contracting volume (R3)	$3(1-\alpha)^{2/3}$	$[1-(1-\alpha)^{1/3}]$
Diffusion models		
1D Diffusion (D1)	$1/2\alpha$	α^2
2D Diffusion (D2)	$[-\ln(1-\alpha)]^{-1}$	$[(1-\alpha)\ln(1-\alpha)]+\alpha$
3D Diffusion-Jander Eq. (D3)	$3(1-\alpha)^{2/3}/2(1-(1-\alpha)^{1/3})$	$[1-(1-\alpha)^{1/3}]^2$
Ginstling–Brounshtein (D4)	$(3/2((1-\alpha)^{-1/3}-1)$	$1-(2\alpha/3)-(1-\alpha)^{2/3}$
Reaction-order models		
Zero-order (F0/R1)	1	α
First-order (F1)	$(1-\alpha)$	$-\ln(1-\alpha)$
Second-order (F2)	$(1-\alpha)^2$	$(1-\alpha)^{-1}-1$
Third-order (F3)	$(1-\alpha)^3$	$0.5[(1-\alpha)^{-2}-1]$

1. They assume a constant kinetic triplet (A, E_a and model).
2. They involve fitting three parameters (A, E_a and model), which are simultaneously determined from a single curve.
3. They involve a single heating rate, which is not always sufficient to determine reaction kinetics.

On the other hand, isoconversional methods calculate E_a at progressive degrees of conversion (α) without modelistic assumptions. The Ozawa, Flynn and Wall method [20,21] is an isoconversional method that utilizes Doyle's linear approximation [9–11] of $p(x)$ (Eq. (10)), which transforms Eq. (10) to,

$$\log \beta = \log \frac{AE_a}{g(\alpha)R} - 2.315 - 0.457\frac{E_a}{RT} \quad (12)$$

A plot of log β versus $1/T$ at each α gives E_a from the slope for a particular α without regard to model.

Vyazovkin and Dollimore [22], utilized a more accurate, non-linear, Senum–Yang [12] approximation of $p(x)$ (Eq. (10)) in their isoconversional method (VYZ), which is based on,

$$\Omega = \left| \sum_{i=1}^{n} \sum_{j \neq i}^{n} \frac{\beta_j I\left(E_{a\alpha}, T_{\alpha i}\right)}{\beta_i I\left(E_{a\alpha}, T_{\alpha j}\right)} \right| \quad (13)$$

where $I(E_{a\alpha}, T_{\alpha i})$ is the exponential integral ($p(x)$) that results from heating rate β_i while $I(E_{a\alpha}, T_{\alpha j})$ is the exponential integral from heating β_j. The activation energy (E_a) is the value that minimizes Ω in Eq. (13) for a particular α.

Vyazovkin modified this method to account for variable heating rates and systematic errors in the activation energy in an advanced isoconversional method (AIC) [23,24] based on the following equation,

$$\Omega = \left| \sum_{i=1}^{n} \sum_{j \neq i}^{n} \frac{J\left(E_{a\alpha}, T_i\left(t_\alpha\right)\right)}{J\left(E_{a\alpha}, T_j\left(t_\alpha\right)\right)} \right| \quad (14)$$

where $J\left(E_a, T(t)\right) = \int_{t_{\alpha-\Delta\alpha}}^{t_\alpha} e^{-E_{a\alpha}/RT(t)} dt$, for a linear heating function: $T(t) = T_0 + \beta t$, in which T_0 is the initial temperature and $\Delta\alpha = (1/m)$ with m being the number of α segments chosen for integration (20 in our work). The integral ($J(E_a, T(t))$) was numerically evaluated by the trapezoidal method. The activation energy (E_a) is the value that minimizes Ω in Eq. (14) for a particular α.

1.2. Varying activation energy

The Arrhenius equation (Eq. (3)) relates the rate constant of a simple one-step reaction to temperature through the activation energy (E_a) and pre-exponential factor (A). It has been traditionally assumed that E_a and A remain constant, however, it has been shown [25–27] that in some solid-state reactions, these kinetic parameters may vary with the progress of the reaction (α). This variation can be detected by isoconversional methods.

Isoconversional methods use several TGA or DSC data sets for kinetic analysis. When performing nonisothermal experiments, care must be taken to ensure that each run is conducted under the same experimental conditions (i.e., sample weight, purge rate, sample size, particle morphology, etc.) so that only the heating rate varies for each run. For example, sample mass varying from one run to another may cause [28]:

a. Variation in endothermic or exothermic effects (i.e., self-heating or self-cooling), inducing deviations from a linear heating rate.
b. Variation in diffusional rates of evolved gases.
c. Thermal gradients varying with sample mass.

Similarly, sample packing could affect solid-state reaction kinetics where loosely packed powders contain larger air pockets that may reduce thermal conductivity or trap evolved gasses compared to a more densely packed powder, which would minimize these effects.

Experimental variation can be minimized, but not totally eliminated. Uncontrolled experimental conditions could cause a thermogram to be altered such that it falls above or below its expected location for a nonisothermal study. This introduces errors in the calculation of the activation energy by isoconversional methods, which are manifested by a false or artifactual variation in activation energy.

In our previous work [5], we tested the sensitivity of different calculational methods isothermally. This work tests the sensitivity of nonisothermal model-fitting and isoconversional methods to similar variables and their application to real TGA data. Actual experimental data was based on desolvation reaction kinetics of a drug solvate (sulfameter). Desolvation reactions are characterized by the removal of solvent molecules from the crystalline solvate below its melting point [29]. Such reaction kinetics can be studied by thermal methods [30].

Sulfameter (structure below) is a long acting sulfonamide that is used for the treatment of urinary tract infections [31]. A dioxolane (structure below) solvate of sulfameter was used to study nonisothermal desolvation reaction kinetics.

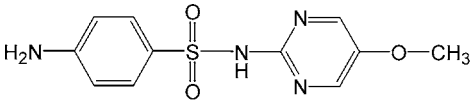

Sulfameter (5–methoxysulfadiazine)
MW – 280.3

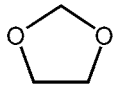

Dioxolane
MW – 74.08

The sulfameter solvate system was selected for this study because it has been previously shown [32] that desolvation of sulfameter solvates is a simple process because solvent molecules fill channels within the crystal structure and desolvation involves the removal of solvent from such channels. Although desolvation does not reflect the inherent complexities observed in many other solid-state systems, it does represent simple solid-state reactions that occur in many pharmaceutical solids.

2. Experimental

This investigation consists of data simulation where several nonisothermal runs were generated then analyzed mathematically and experimental results for the nonisothermal desolvation of sulfameter-dioxolane solvate.

Nonisothermal kinetic data were evaluated by model-fitting methods (Coats–Redfern) in addition to isoconversional methods, which include the Ozawa–Flynn–Wall (OFW) method and Vyazovkin's (VYZ) isoconversional and advanced isoconversional (AIC) methods.

2.1. Data simulation

A simple, one-step reaction (solid A producing solid B and gas C) according to the scheme below was simulated nonisothermally:

$$A_{(s)} \rightarrow B_{(s)} + C_{(g)}$$

Twenty-four simulations were generated using Microsoft® Excel from the integral form of the rate law (Eq. (10)). Nonisothermal data were simulated by calculating the temperature (T) for α values between 0.01 and 0.99 according to:

$$\Psi = \left| g(\alpha)\frac{\beta R}{A E_a} - p(x) \right| \quad (15)$$

Values were assigned to the above parameters ($g(\alpha)$, E_a, A and β) and the exponential integral ($p(x)$) was approximated by the 3rd degree Senum–Yang approximation. Nonisothermal data were simulated using Microsoft Excel's Solver® by finding the value of T at each α, which minimizes Ψ in Eq. (15).

Nonisothermal runs were simulated in two data sets (sets B and C). The first simulation in set B (B1) consisted of five error-free nonisothermal (α–T) curves generated at five heating rates (2, 4, 8, 16 and 32 K/min) using a first-order model ($g(\alpha) = -\ln(1-\alpha)$) with $A = 1 \times 10^{15}$ min^{-1} and E_a = 100 kJ/mole (Fig. 1a). Thirteen additional simulations (B2–14) were generated from B1 using the same kinetic parameters and model but with perturbations in temperature or heating rate (Table 2)

The first simulation in set C (C1) consisted of five error-free nonisothermal (α–T) curves, which were generated using the same parameters for simulation B1 except the heating rates (0.5, 1, 1.5, 2 and 2.5 K/min) (Fig. 1b) covered a narrower range. Nine additional simulations (C2–10) were generated from C1 using the same kinetic parameters and model but with different perturbations in each (Table 2). The use of low heating rates as in simulation set C has been previously suggested [33] to narrow the temperature range of nonisothermal experiments. Narrow temperature ranges may reduce differences between isothermal and nonisothermal experiments [33].

Ideally, perturbations should affect all α–T curves, but many more simulations would have to be generated and it would be difficult to determine the particular effect of the perturbation on a α–T curve. Alternatively, perturbations were introduced into one or two α–T curves to precisely observe their effect on the kinetic results.

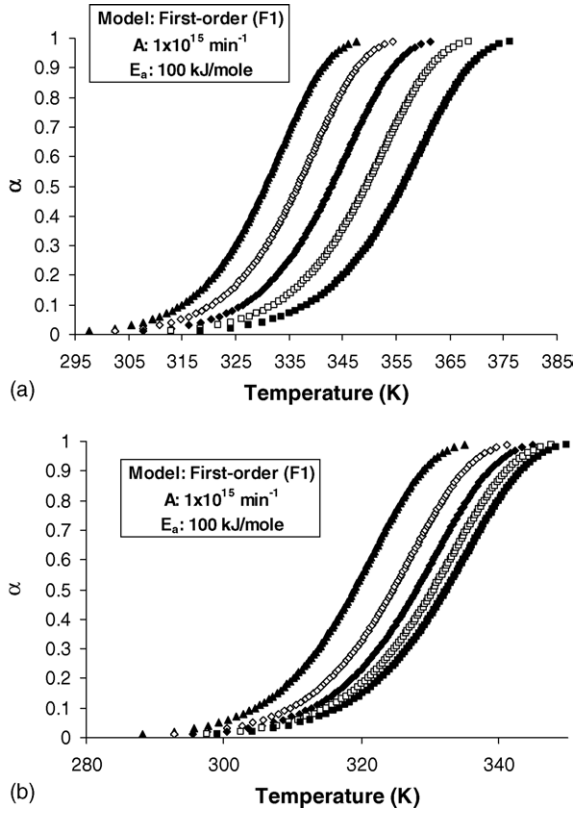

Fig. 1. Error-free simulations (B1, C1) of α vs. temperature for nonisothermal kinetic runs at: (a) (▲) 2 K/min; (◊) 4 K/min; (♦) 8 K/min; (□) 16 K/min and (■) 32 K/min (simulation B1); (b) (▲) 0.5 K/min; (◊) 1 K/min; (♦) 1.5 K/min; (□) 2 K/min and (■) 2.5 K/min (simulation C1). The inset gives the model, pre-exponential factor (A) and activation energy (E_a) for these simulations.

Perturbations introduced into each simulation set included shifting one or more curves or changing their nominal heating rate. A curve shift simulates thermal lag in a sample, while a change in the nominal heating rate simulates possible self-cooling/heating effects or the effect of using the programmed heating rate rather than the actual one.

Kinetic analysis of each simulation was done by the Coats–Redfern model-fitting method [13,14] in addition to several isoconversional methods: Ozawa–Flynn–Wall [20,21]; Vyazovkin's isoconversional [22]; and, the advanced isoconversional [23,24]. All kinetic analyses were conducted with Microsoft Excel's Solver® tool for the Vyazovkin and AIC methods or direct calculation for the OFW and Coats–Redfern methods.

2.2. Sulfameter solvate desolvation

Sulfameter was obtained from Sigma® Chemical Co. (lot no. 107F0910) while dioxolane was obtained from Aldrich®

Table 2
Nonisothermal simulations generated from simulations B1, C1 (error-free), produced using a first-order reaction model (F1) with, $A = 1 \times 10^{15}\ \text{min}^{-1}$ and $E_a = 100$ kJ/mol

Simulation	Simulation characteristics*
B1	Five nonisothermal curves at heating rates of 2, 4, 8, 16 and 32 K/min
B2	32 K/min curve shifted by +2 K
B3	32 K/min curve shifted by −2 K
B4	16 K/min curve shifted by −2 K
B5	8 K/min curve shifted by −2 K
B6	4 K/min curve shifted by −2 K
B7	1 K/min curve shifted by −2 K
B8	Heating rate of 32 K/min curve taken as 28.2 K/min
B9	Heating rate of 16 K/min curve taken as 14.4 K/min
B10	Heating rate of 8 K/min curve taken as 7.2 K/min
B11	Heating rate of 4 K/min curve taken as 3.6 K/min
B12	Heating rate of 2 K/min curve taken as 1.8 K/min
B13	2 K/min and 32 K/min curves shifted by +3 K and −2 K, respectively
B14	0.5% random error in temperature (°C) added to each curve
C1	Five nonisothermal curves at heating rates of 0.5, 1, 1.5, 2 and 2.5 K/min
C2	0.5 K/min curve shifted by +2 K
C3	1 K/min curve shifted by +2 K
C4	1.5 K/min curve shifted by +2 K
C5	2 K/min curve shifted by +2 K
C6	2.5 K/min curve shifted by +2 K
C7	0.5 K/min curve shifted by −2 K
C8	1.5 K/min curve shifted by −2 K
C9	2.5 K/min curve shifted by −2 K
C10	0.5% random error in temperature (°C) added to each curve

* Simulations B2–13 and C2–10 are perturbations of B1 and C1 simulations, respectively.

Chemical Co. (lot no. LO14921KO). These chemicals were used as supplied. A dioxolane solvate of sulfameter was prepared by recrystallizing sulfameter from the neat solvent. Samples were sieved and a particle size range of 850–1700 μm was used.

Desolvation data for the solvate was obtained nonisothermally by thermogravimetry using a Perkin-Elmer TGA 7. The TGA temperature was calibrated by a two-point calibration method using alumel and nickel. A flow of nitrogen gas ranging from 40 to 50 ml/min was used as a purge.

Five data sets, each containing five samples of sulfameter-dioxolane were desolvated at different heating rates. Sample sizes ranged from 3 to 5 mg. Within each set, sample weights were within 5% of each other. Runs were performed at nominal heating rates of 1, 1.5, 2, 2.5 and 3 K/min for two sets while nominal heating rates for the remaining three sets were 1, 2, 4, 8 and 16 K/min. The exact heating rate was obtained from the slope of the linear heating curve of the TGA run during the time period of significant weight loss.

Kinetic analysis for desolvation data was done by model-fitting and isoconversional methods, as described earlier for simulated data.

3. Results and discussion

Fig. 2 shows five sets of nonisothermal desolvation thermograms for sulfameter-dioxolane samples. Gravimetric weight loss for these solvates showed a 1:1 drug–solvent ratio (∼21% w/w). Kinetic analysis for simulated and real data sets is described below.

3.1. Simulated data

3.1.1. Isoconversional methods

Kinetic results for nonisothermal data (Figs. 3–9) show the sensitivity of isoconversional methods to introduce perturbations. This sensitivity is manifested either as an inaccurate value of E_a or as an artifactual variation in E_a as a function of α.

Perturbations involving curve shifts had two effects on kinetic analysis. First, calculated E_a values were significantly affected and second, the linearity of isoconversional plots was affected producing an artifactual variation in E_a. These effects were seen for both simulation sets B (B2–7, Fig. 4; B13, Fig. 5) and C (C2–9, Fig. 8).

Perturbations, which changed the heating rate did not affect the shape (i.e., linearity) of the isoconversional (E_a–α) plot. However, they significantly changed calculated E_a values, as seen in simulations B8–12 (Fig. 5).

Analysis of simulation results also showed that the same perturbation had different effects on each curve, which has been previously shown isothermally [5]. In simulation set B, perturbations affecting the middle curve (3rd of five) produced less error than those affecting the outer curves (i.e., 1st or 5th curve). For example, in simulations B3 and B7 (Fig. 4), shifting an outer curve (1st or 5th) by −2 K produced a larger error in E_a compared to simulation B5 with the same shift on a middle curve (∼6% versus 0.8%). A similar observation is seen for simulations B8 and B12 where a larger error in E_a was produced when an outer curve was shifted compared to less error for B10, which involved a shift in the middle curve (∼3% versus <0.1%, Fig. 5). The maximum error in E_a was produced in simulation B13 where more than one curve was shifted (∼18% Fig. 5).

For simulation set C, fitted results also showed that perturbations affecting outer curves (i.e., 1st or 5th) produced higher E_a variation than those affecting the middle curve (i.e., 3rd). However, errors in E_a differed if the direction of the perturbation changed (Fig. 8). For example, simulations C2 and C6, involved shifting the first (C2) and fifth (C6) curves by +2 K or −2 K, respectively, gave ∼16% error in E_a (C2) compared to ∼10% error (C6). Similarly, C2 and C7 involved shifting the first curve (0.5 K/min curve) by +2 K and −2 K, respectively, producing ∼16% (C2) compared to ∼14% (C7) errors in E_a. Also, C4 and C8 involved shifting the 3rd curve (1.5 K/min curve) by +2 K and −2 K, respectively, producing errors of ∼4.5% (C4) or ∼0.7% (C8).

Errors produced in simulation set C were generally higher than those in set B. For example, a curve shift of −2 K for

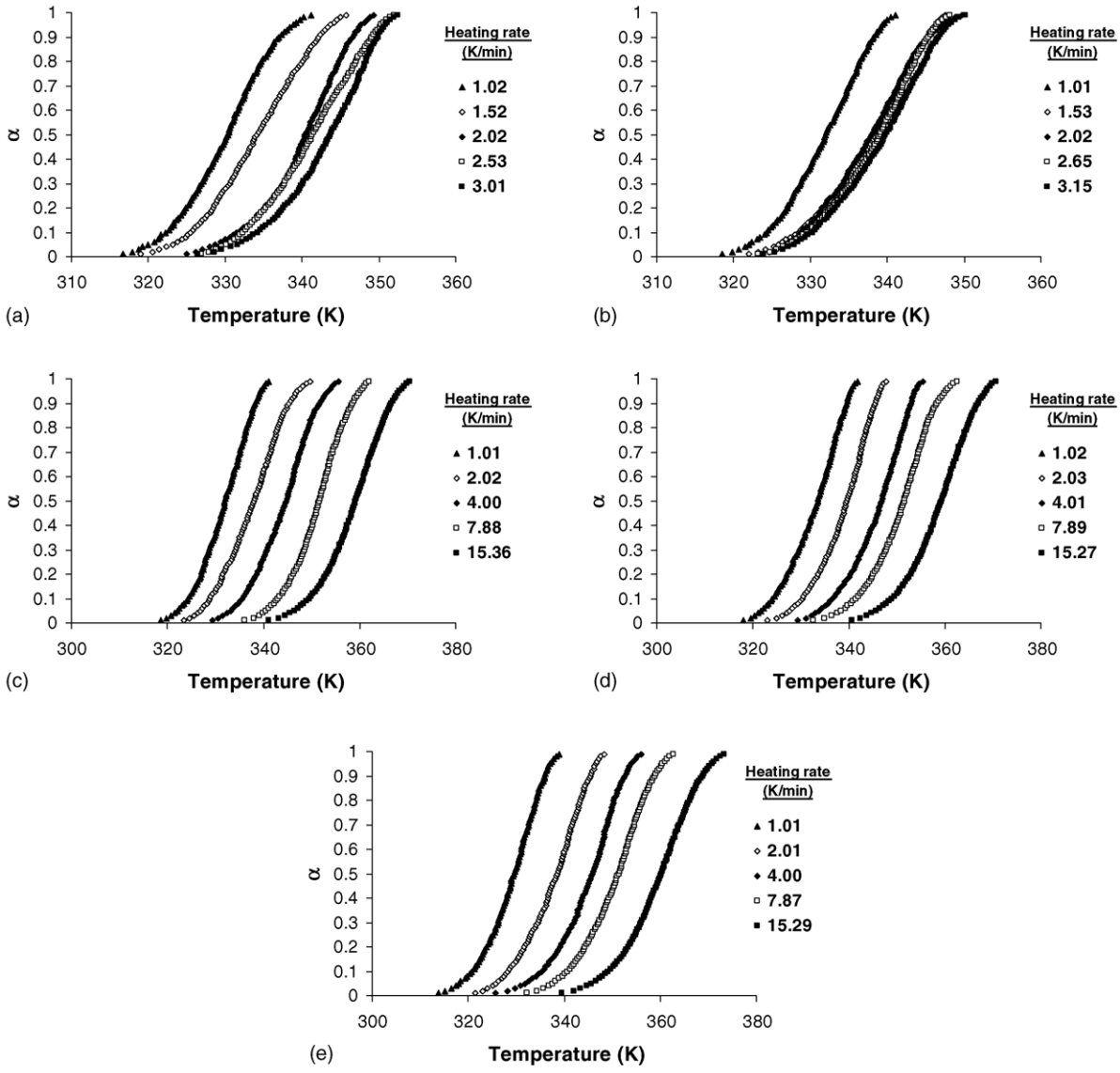

Fig. 2. α–T plots for the nonisothermal desolvation of sulfameter-dioxolane solvate sets: (a) set 1; (b) set 2; (c) set 3; (d) set 4; (e) set 5.

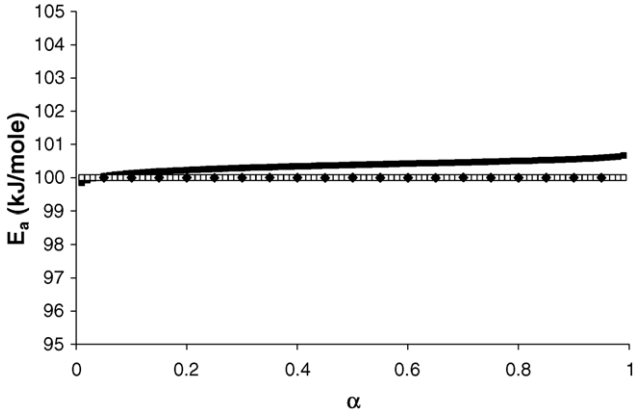

Fig. 3. E_a–α plots of simulated nonisothermal runs (simulation B1), evaluated by three isoconversional methods: (□) VYZ; (■) OFW; (⧫) AIC.

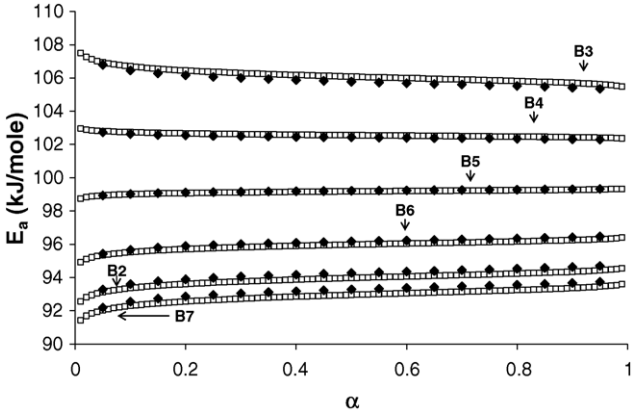

Fig. 4. E_a–α plots of simulated nonisothermal runs (simulations B2–7), evaluated by two isoconversional methods: (□) VYZ; (⧫) AIC.

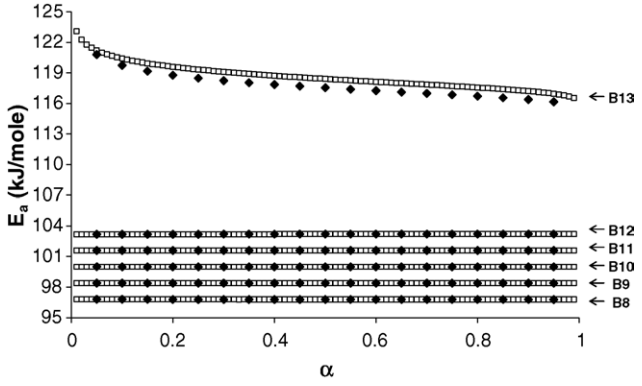

Fig. 5. E_a–α plots of simulated nonisothermal runs (simulations B8–13), evaluated by two isoconversional methods: (□) VYZ; (⧫) AIC.

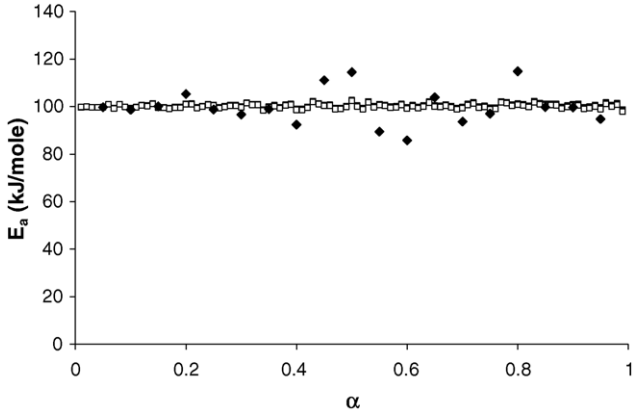

Fig. 6. E_a–α plots of simulated nonisothermal runs (simulation B14), evaluated by three isoconversional methods: (□) VYZ; (■) OFW; (⧫) AIC.

the first curve in simulations B7 and C7 produced an E_a error of ∼7% (B7) versus ∼14% (C7). Shifting the last curve by +2 K and −2 K in B2 and B3 produced ∼6% error in E_a for each. However, these shifts (+2 K and −2 K in the last curve) produced E_a errors ∼10% (C6) and 8% (C9) in set C. Larger errors in simulations C are probably due to the experimental design. In this simulation set (set C), heating rates were

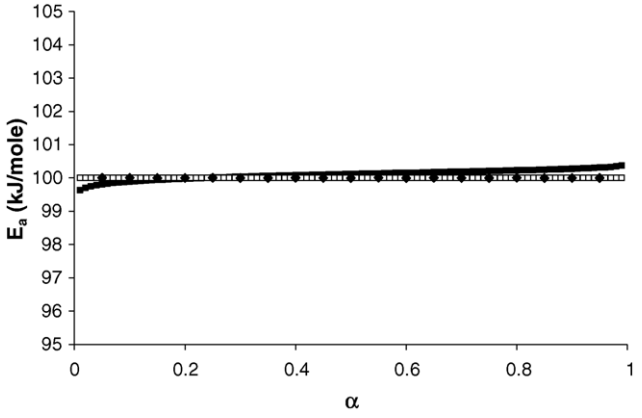

Fig. 7. E_a–α plots of simulated nonisothermal runs (simulation C1), evaluated by three isoconversional methods: (□) VYZ; (■) OFW; (⧫) AIC.

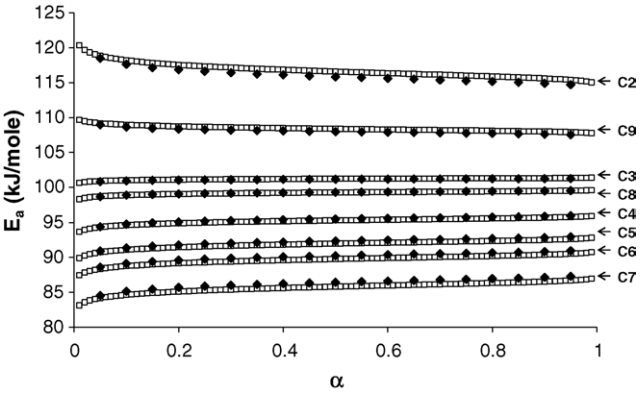

Fig. 8. E_a–α plots of simulated nonisothermal runs (simulations C2–9), evaluated by two isoconversional methods: (□) VYZ; (⧫) AIC.

selected to yield curves that cover a narrower temperature range, which produced curves less separated than those over the wider temperature range in simulation set B. For example, C1 curves were closely spaced (Fig. 1b) with each curve separated by the 0.5 K/min difference in heating rate (i.e., 0.5, 1, 1.5, 2 and 2.5 K/min), whereas, curves in simulation B1 (Fig. 1a) were separated by a two-fold heating rate difference (i.e., 2, 4, 8, 16 and 32 K/min). As a result, any curve shift is likely to affect closely spaced curves (set C) more than widely spaced ones (set B).

Because narrow temperature-range curves are so closely spaced, any shift within these curves may cause a curve to shift to a position where it overlaps the curve that follows it (i.e., curve having a higher heating rate) or overlaps the curve that precedes it (i.e., curve having a lower heating rate). This overlap was observed in simulations C4 (1.5 and 2 K/min curves), C5 and C9 (2 and 2.5 K/min curves) as seen in Fig. 10a–c, but this effect is less likely in wider temperature-range curves as they are more widely spaced. Even when maximal curve shifts were introduced (B13), simulated curves remained well separated (Fig. 10d).

Data analysis also showed that the AIC method was slightly more accurate in calculating E_a than the OFW or

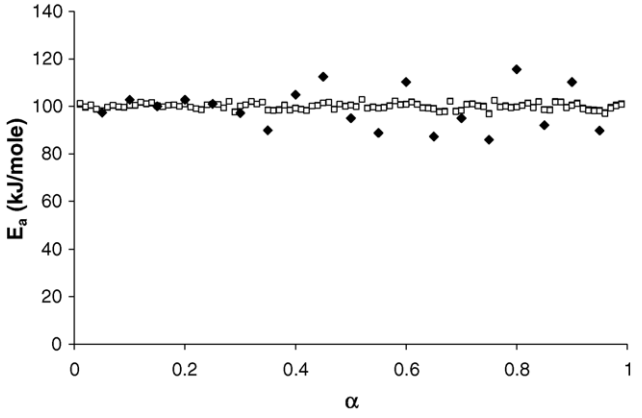

Fig. 9. E_a–α plots of simulated nonisothermal runs (simulation C10), evaluated by three isoconversional methods: (□) VYZ; (■) OFW; (⧫) AIC.

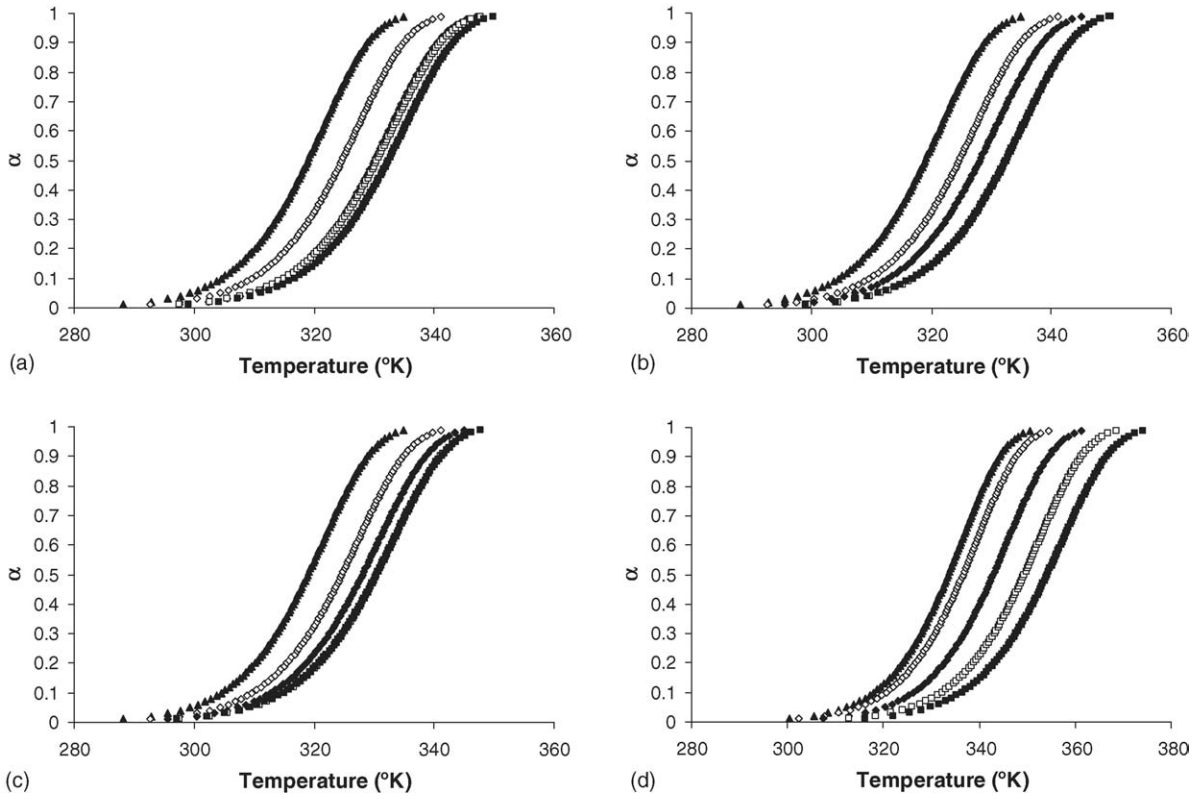

Fig. 10. α–T curves for simulations C4, C5 and C9 (a–c) at nominal heating rates of: (▲) 2 K/min; (◊) 4 K/min; (♦) 8 K/min; (□) 16 K/min; (■) 32 K/min and simulation B13; (d) at: (▲) 0.5 K/min; (◊) 1 K/min; (♦) 1.5 K/min; (□) 2 K/min and (■) 2.5 K/min.

VYZ methods, however, it was more sensitive to random errors (Figs. 6 and 9). The higher random error is probably due to integration over small α intervals ($\Delta\alpha = 0.05$) in Eq. (14); the scatter could be reduced by smoothing but experimental information could be lost if too much smoothing is done.

3.1.2. Model-fitting results

Kinetic analysis of simulated data by the Coats–Redfern model-fitting method shows that perturbations introduced little effect on calculated kinetic parameters (Table 3) as A and E_a were calculated with little error. However, two problems were encountered: all models gave acceptable fits ($r > 0.93$); some models were indistinguishable (A2, A3, A4 and F1) based on quality of the fit (i.e., all r-values equal). Therefore, quality of fit is a poor indicator of the best model when using model-fitting methods, as other authors have reported [33].

3.2. Sulfameter desolvation

Fig. 11 shows E_a–α plots for the desolvation of five experimental data sets for sulfameter-dioxolane solvate desolvation. The isoconversional plots of all sets show variation in E_a. Sample sets 1–2 (Fig. 11a and b) show the highest random scatter (AIC method) and systematic variation in E_a. The isoconversional plots for the two sets were also

Table 3
Fitted kinetic parameters for simulated nonisothermal data (B and C), using the Coats–Redfern method[a,b]

Simulation	A (min^{-1}) × 10^{14}	E_a (kJ/mol)
B1	9.5	99.9
B2	10.0	100.1
B3	9.2	99.6
B4	9.1	99.6
B5	9.1	99.6
B6	9.1	99.6
B7	9.1	99.6
B8	9.3	99.9
B9	9.3	99.9
B10	9.3	99.9
B11	9.3	99.9
B12	9.3	99.9
B13	9.8	100.0
B14	9.7	99.9
C1	9.6	99.9
C2	10.1	100.1
C3	10.0	100.1
C4	10.0	100.1
C5	10.0	100.1
C6	10.0	100.1
C7	9.1	99.6
C8	9.1	99.6
C9	9.1	99.6
C10	9.4	99.8

[a] Results shown for first-order (F1) model.
[b] Results averaged from five heating rate curves using the geometric mean of A and E_a.

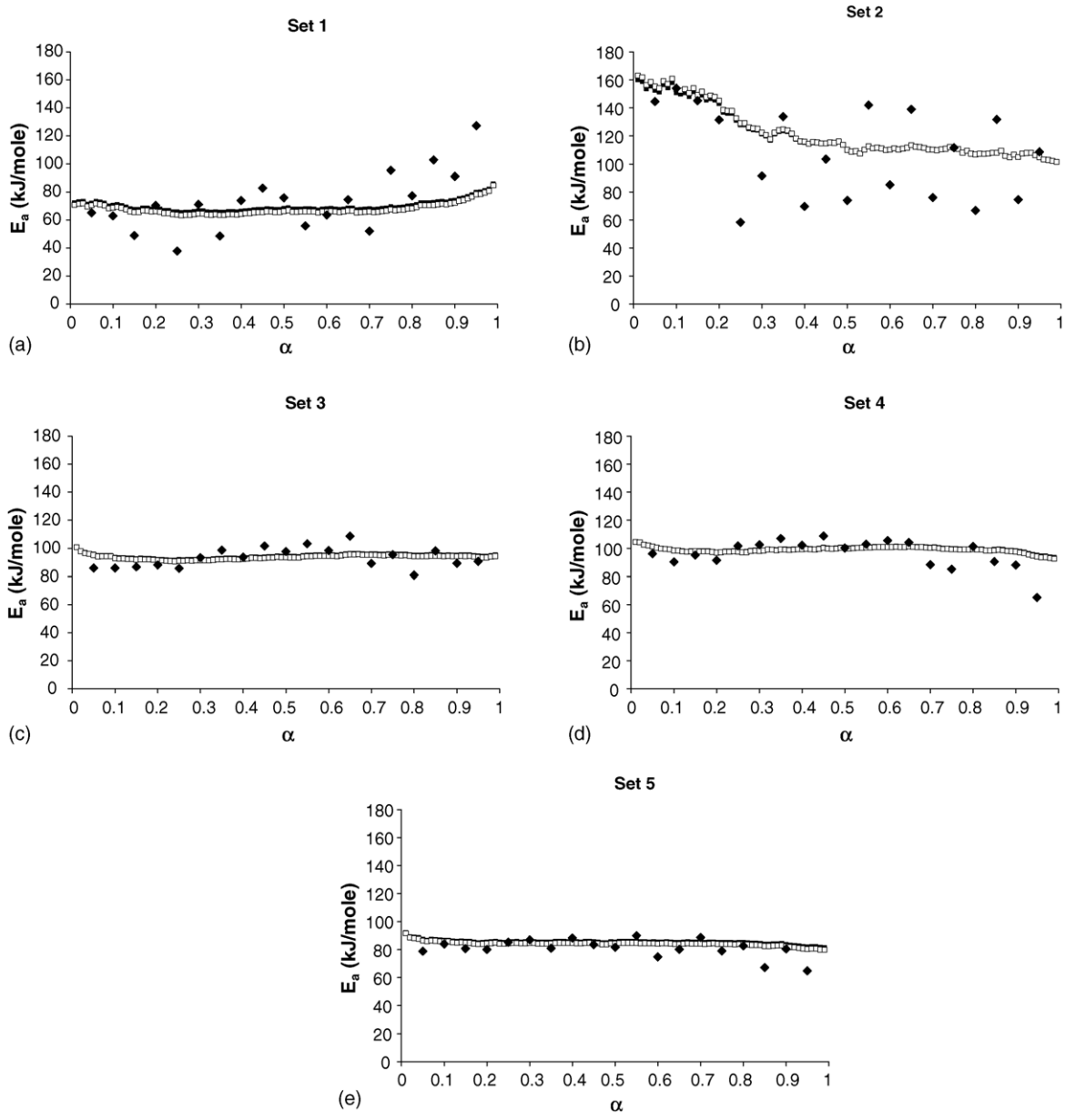

Fig. 11. E_a–α plots for nonisothermal sulfameter-dioxolane solvate desolvation runs (sets 1–5), evaluated by three isoconversional methods: (■) OFW; (□) VYZ; (⧫) AIC.

significantly different, especially for $\alpha < 0.5$ (Fig. 12). On the other hand, sample sets 3–5 (Fig. 11c–e) showed less systematic E_a variation and random scatter. However, the isoconversional plots for all three data sets were comparable (Fig. 12) indicating better consistency of more widely spaced heating rates.

Isoconversional plots for sets 1–2 are comparable to those for simulation set C as they involve heating rates that produce closely spaced curves (i.e., cover a narrow temperature range) while plots for sets 3–5 are comparable to those obtained from simulation set B as they involve heating rates that produce widely spaced curves (i.e., cover a wider temperature range). Large errors seen in sample sets 1–2 compared to sets 3–5 are perhaps due to the nature of the experimental protocol as was seen for simulation set C. Like simulation C1, curves in sample sets 1–2 were closely spaced where small curve shifts in these sets caused their positions to move above or below their expected positions (Fig. 13a), which dramatically affects the shape of isoconversional plots (Fig. 12). Similarly, simulation B1 resembles those of sample sets 3–5 as they were widely spaced and curve shifts due to experimental variation had less effect on curve positions (Fig. 13b) and the shape of isoconversional plots (Fig. 12).

Also, experimental TGA curves are generally expected to produce more errors in the isoconversional kinetic analysis

Table 4
Fitted kinetic parameters for nonisothermal sulfameter-dioxolane desolvation data sets (Fig. 2), using the Coats–Redfern method[a]

Model	ln A (min^{-1})					E_a (kJ/mol)				
	Set 1	Set 2	Set 3	Set 4	Set 5	Set 1	Set 2	Set 3	Set 4	Set 5
A2	30.5	30.1	31.9	30.6	28.4	91.0	89.6	94.5	91.2	84.7
A3	18.7	18.5	19.9	19.0	17.5	58.8	57.9	61.1	58.9	54.5
A4	12.8	12.6	13.8	13.1	12.0	42.7	42.0	44.4	42.7	39.5
D1	97.3	96.2	99.6	97.1	90.3	279.8	276.0	289.8	283.6	263.3
D2	106.3	105.0	108.7	105.7	98.3	305.9	301.8	317.1	309.2	287.3
D3	117.7	116.3	120.5	116.5	108.5	341.3	336.4	354.0	343.6	319.7
D4	109.0	107.7	111.5	108.2	100.6	317.4	313.0	329.1	320.4	297.8
F1	65.4	64.6	67.3	64.8	60.4	187.6	184.8	194.8	188.1	175.0
F2	94.0	92.7	96.7	91.8	86.1	265.2	260.8	276.3	263.0	245.8
F3	129.7	127.8	133.5	125.5	118.1	362.7	356.2	378.7	356.9	334.7
P2	21.0	20.8	22.1	21.5	19.8	65.7	64.8	68.2	66.6	61.6
P3	12.3	12.1	13.3	12.9	11.7	42.0	41.3	43.5	42.5	39.1
P4	7.9	7.8	8.8	8.5	7.6	30.1	29.6	31.2	30.5	27.9
R1	46.7	46.1	48.2	46.9	43.5	137.1	135.2	142.0	139.0	128.8
R2	54.2	53.5	55.9	54.1	50.2	159.1	156.9	165.0	160.5	149.0
R3	57.0	56.3	58.8	56.7	52.7	167.8	165.4	174.1	168.9	157.0

[a] Results in each data set are averaged from five heating rate curves (geometric mean of E_a and A).

because, in addition to any observed curve shift that might occur, actual heating rates are usually different from those programmed due to self-heating/cooling effects. Therefore, in reality, curves are more tightly spaced than expected in the experimental protocol.

Model-fitting results of sample sets showed that kinetic parameters (E_a and A) of all sets gave comparable values for each model (Table 4). Therefore, curve shifts that occurred from different experimental variables had less effect on kinetic parameters calculated by the Coats–Redfern method. This finding was also substantiated by the analysis of simulated data. Problems encountered with the Coats–Redfern model-fitting method were similar to those seen for simulated data, which included excellent fits for all models ($r > 0.94$, Fig. 14) with some models being indistinguishable (A2, A3, A4 and F1) based on a statistical criterion (see variation in r for each model, Fig. 14).

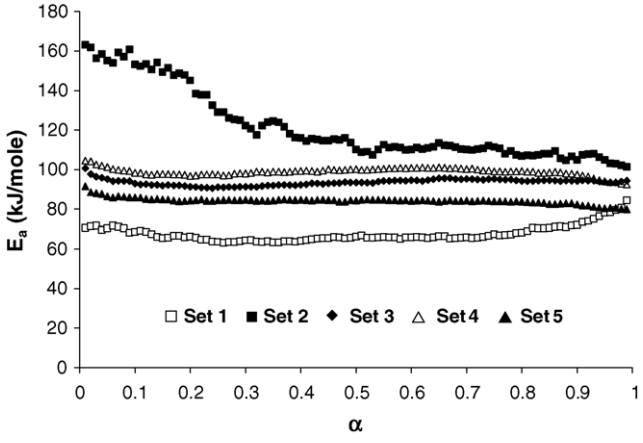

Fig. 12. E_a–α plots for nonisothermal sulfameter-dioxolane solvate desolvation evaluated by the Vyazovkin (VYZ) method.

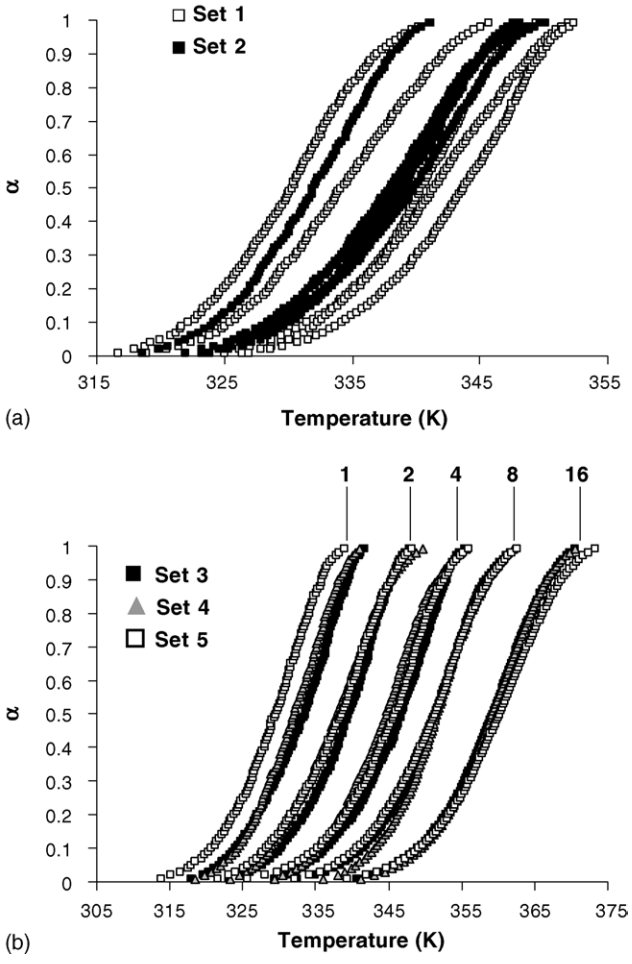

Fig. 13. α–T plots for the nonisothermal desolvation of sulfameter-dioxolane solvate for five experimental sets: (a) sets 1–2 with nominal heating rates of 1, 1.5, 2, 2.5 and 3 K/min; (b) sets 3–5 with nominal heating rates of 1, 2, 4, 8 and 16 K/min.

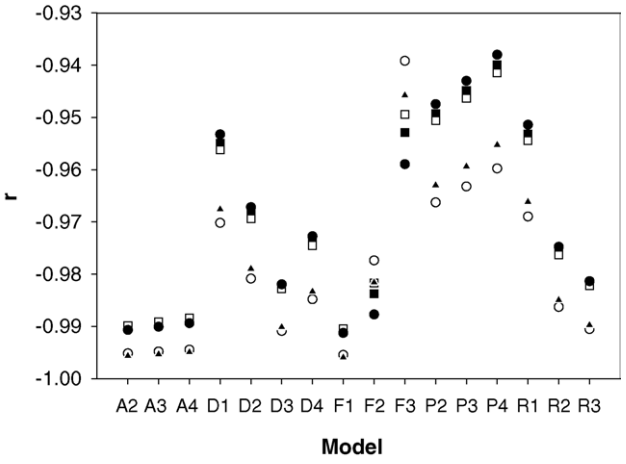

Fig. 14. Model-fitting correlation coefficients (r) for nonisothermal sulfameter-dioxolane solvate desolvation evaluated by the Coats–Redfern method: (■) set 1; (□) set 2; (●) set 3; (○) set 4; (▲) set 5. Values from each set are averaged from five curves.

4. Conclusions

Reaction complexity in solid-state kinetics is usually described by a variation in E_a as a reaction proceeds and this variation is best detected by isoconversional methods that perform a model-free analysis of E_a as a function of conversion. However, our results showed methods that detect reaction complexity can also artificially contribute to this complexity, which is manifested as an artifactual E_a variation. An artifactual variation in E_a can result in erroneous mechanistic conclusions about a reaction being complex when, in fact, it is not.

Isothermally, most isoconversional methods do not contribute to this artifactual variation [5], however, nonisothermal results showed that all tested isoconversional methods produced artifactual variation in E_a. This variation was of different magnitudes compared to true variations that result from reaction complexity, while the magnitude of this variation appears to be small compared to the actual E_a variation (i.e., resulting from reaction complexity) in some experiments where curves were well separated, the magnitude of artifactual variation was quite high in others, which had little separation between curves.

Artifactual E_a variation can be attributed to various experimental variables that can shift thermogravimetric curves from their expected positions (e.g., less systematic shift with increasing heating rate), which are manifested as variations in E_a with isoconversional analysis methods. Such variations in E_a will be observed in all isoconversional methods because they are related to the quality of experimental data rather than to the methods themselves. Therefore, such a variation cannot be reduced or prevented in any isoconversional method unless more careful control of experimental variables and better experimental design are applied. Control of experimental variables can be achieved by using the same particle size (i.e., sieving) for each solid sample, using the same weight for each run (±5%), controlling purge gas flow rate as well as carefully replicating experiments. Nonisothermal experiments should be designed so that curves are widely separated. A two-fold difference in heating rates between curves produced more consistent E_a values in our experimental work.

Model-fitting methods were least affected by experimental variables that cause curve shifts. However, they simultaneously determine E_a and A from a single thermogravimetric curve, which could lead to inaccuracies, such as indistinguishable models based on statistical criteria. Additionally, model-fitting methods cannot reveal reaction complexity as they assume a constant value of E_a and A, which may be a valid assumption for the sulfameter solvate system, it has been previously shown that desolvation of this type of solvate is a simple reaction [32] that could be described by a single kinetic triplet (A, E_a and model) [34].

Inaccurate determination of heating rates affects all calculation methods in solid-state kinetic analyses. Therefore, the actual heating rate of each run rather than that programmed should be used in kinetic analyses.

Finally, there is no single method that can perfectly evaluate solid-state kinetics, even for a simple system, such as desolvation. Both modelistic and model-free methods have their advantages and limitations. An approach that utilizes both methods in a complementary fashion has been shown to produce promising results. Such an approach is recommended for the evaluation of simple solid-state kinetics [34].

References

[1] M.E. Brown, J. Therm. Anal. 49 (1997) 17.
[2] A.K. Galwey, M.E. Brown, J. Therm. Anal. 60 (2000) 863.
[3] A.K. Galwey, Thermochim. Acta 397 (2003) 249.
[4] S. Vyazovkin, Thermochim. Acta 397 (2003) 269.
[5] A. Khawam, D.R. Flanagan, Thermochim. Acta 429 (2005) 93.
[6] K.J. Laidler, J. Chem. Educ. 61 (1984) 494.
[7] A.K. Galwey, M.E. Brown, Thermal Decomposition of Ionic Solids: Chemical Properties and Reactivities of Ionic Crystalline Phases, second ed., Elsevier, Amsterdam, 1999, p. 75.
[8] J.H. Flynn, Thermochim. Acta 300 (1997) 83.
[9] C.D. Doyle, J. Appl. Polym. Sci. 5 (1961) 285.
[10] C.D. Doyle, J. Appl. Polym. Sci. 6 (1962) 639.
[11] C.D. Doyle, Nature 207 (1965) 290.
[12] G.I. Senum, R.T. Yang, J. Therm. Anal. 11 (1977) 445.
[13] A.W. Coats, J.P. Redfern, Nature 201 (1964) 68.
[14] A.W. Coats, J.P. Redfern, J. Polym. Sci. B: Polym. Lett. 3 (1965) 917.
[15] M.E. Brown, M. Maciejewski, S. Vyazovkin, R. Nomen, J. Sempere, A. Burnham, J. Opfermann, R. Strey, H.L. Anderson, A. Kemmler, R. Keuleers, J. Janssens, H.O. Desseyn, C.R. Li, T.B. Tang, B. Roduit, J. Malek, T. Mitsuhashi, Thermochim. Acta 355 (2000) 125.
[16] A.K. Burnham, Thermochim. Acta 355 (2000) 165.
[17] M. Maciejewski, Thermochim. Acta 355 (2000) 145.
[18] B. Roduit, Thermochim. Acta 355 (2000) 171.
[19] S. Vyazovkin, Thermochim. Acta 355 (2000) 155.
[20] T. Ozawa, Bull. Chem. Soc. Jpn. 38 (1965) 1881.
[21] J.H. Flynn, L.A. Wall, J. Polym. Sci. B: Polym. Lett. 4 (1966) 323.
[22] S. Vyazovkin, D. Dollimore, J. Chem. Inf. Comput. Sci. 36 (1996) 42.
[23] S. Vyazovkin, J. Comput. Chem. 22 (2001) 178.

[24] S. Vyazovkin, J. Comput. Chem. 18 (1997) 393.
[25] S. Vyazovkin, Int. Rev. Phys. Chem. 19 (2000) 45.
[26] S. Vyazovkin, New J. Chem. 24 (2000) 913.
[27] S. Vyazovkin, C.A. Wight, Annu. Rev. Phys. Chem. 48 (1997) 125.
[28] W.W. Wendlandt, Thermal Analysis, third ed., Wiley, New York, 1986, p. 33.
[29] S.R. Byrn, R.R. Pfeiffer, J.G. Stowell, Solid-State Chemistry of Drugs, second ed., SSCI Inc., West Lafayette, 1999, p. 279.
[30] M.E. Brown, Introduction to Thermal Analysis: Techniques and Applications, second ed., Kluwer Academic Publishers, 2001.
[31] C.O. Wilson, O. Gisvold, R.F. Doerge, Textbook of Organic Medicinal and Pharmaceutical Chemistry, eighth ed., Lippincott, Philadelphia, 1982, p. 197.
[32] M.R. Caira, R. Mohamed, Supramol. Chem. 2 (1993) 201.
[33] S. Vyazovkin, C.A. Wight, J. Phys. Chem. A 101 (1997) 8279.
[34] A. Khawam, D.R. Flanagan, J. Phys. Chem. B 109 (2005) 10073.